JOURNAL OF MATERIALS SCIENCE 30 (1995) 5215–5222

Interfacial reactions in the liquid diffusion couples of Mg/Ni, Al/Ni and Al/(Ni)–Al_2O_3 systems

CHUN-LIN TSAO, SINN-WEN CHEN
Department of Chemical Engineering, National Tsing-Hua University Hsin-Chu, Taiwan 30043

The interfacial reactions between various molten metals and solid plates were investigated in this diffusion couple study. The molten metals were pure magnesium, pure aluminium, aluminium-rich Al–Mg alloy, and aluminium-rich Al–Cu alloys, and the solid plates were pure nickel plate, alumina plate, and nickel-plated alumina plate. The interfacial reactions in the diffusion couples were determined by using optical microscopy, scanning electron microscopy and electron probe microanalysis in regard to the formation of intermetallic phases, the dissolution rates of the nickel plates, and the morphology of the interfaces. Mg_2Ni phase was found in the pure Mg/Ni plate diffusion couples, and the Al_3Ni and Al_3Ni_2 phases were observed in the pure Al/Ni plate and Al-alloys/Ni plate diffusion couples. In the Al–Cu alloy/Ni-plated alumina plate diffusion couple, Al_2O_3 formed at the interface, while spinel particles were found in the diffusion couples of Al–7.4 wt% Mg alloy/Ni-plated alumina plate. Experimental difficulty was encountered in preparing the diffusion couples with alumina plate, and a gap existing at the interface prohibited reactions between the molten metal with alumina plate.

1. Introduction

Alumina-reinforced aluminium matrix composites have received much interest owing to their high strength to density ratio, high Young's modulus to density ratio, and their good interfacial stability [1–4]. The wetting ability between the aluminium alloys and the alumina is poor. The addition of some active elements, such as magnesium, to alloys and surface treatments of alumina, such as nickel plating, are the most common treatments used to overcome this non-wetting difficulty [5–7]. The improvement of the wetting ability mainly results from the chemical reactions between the added elements with the substrate and the surface coating with the molten alloy. In this study, the interfacial reactions between various molten metals and solid plates were investigated. The molten metals were pure aluminium, pure magnesium, aluminium-rich Al–Cu alloys, and aluminium-rich Al–Mg alloys, and the solid plates were nickel plate, alumina plate, and nickel-plated alumina plate.

The reactions between the molten aluminium alloys and the alumina have been investigated by many researchers [1, 6, 8–14]. Levi *et al.* [1] studied the interfacial reactions between polycrystalline alumina fibres and several aluminium-rich alloys. They found a stable Al_2MgO_4 spinels formed at the interface of alumina fibre and Al–Mg alloys, and the spinel formation was also observed by many other research groups [6, 8, 9, 12–14]. The studies of the interfacial reactions between the molten aluminium alloys and alumina are summarized in Table I. In spite of the frequent observation of the spinel formation, Cappleman *et al.* [10] carried out their experiments in a shorter time (only for a few minutes), but did not find any spinel in their samples. Weirauch's experimental results [6] indicated that the spinel formed in the systems with higher magnesium content aluminium alloys (Al–6.0 wt % Mg), but not in those with lower magnesium content alloys (Al–3.0 wt % Mg). Besides the formation of Al_2MgO_4 spinel at the interface, Levi *et al.* [1] and Molins *et al.* [12] also found the MgO phase, yet it was not reported by other researchers [6, 8–11, 13, 14]. The formation rates of spinel were seldom discussed, and the results reported by Levi *et al.* [1], Molins *et al.* [12], and McLeod and Gabryel [14] were scattered. Later in this report we will discuss the experimental difficulties encountered in this study when investigating the interfacial reactions between the molten aluminium alloys and alumina, which might explain the inconsistency of the data in the literature.

Besides the addition of magnesium to aluminium alloys, nickel plating of the alumina can also enhance the wetting ability, and this is mainly due to the plated nickel reacting with the molten aluminium. According to the Al–Ni equilibrium phase diagram [15], four phases, Al_3Ni, Al_3Ni_2, AlNi, and $AlNi_3$, are likely to form at the Al/Ni interface when annealed below 854 °C. Castleman and Seigle [16, 17] prepared Al/Ni diffusion couples annealed from 400–625 °C, and they determined only Al_3Ni, Al_3Ni_2 phases at the Al/Ni interface. There were very thin layers of the AlNi and $AlNi_3$ phases found in the Al/Ni diffusion couples with long-term annealing, 340 h, at 600 °C. Janssen

0022–2461

TABLE I Interactions between the molten aluminium alloys and alumina

System	Experimental conditions	Experimental results	Reference
Al–Mg/Al_2O_3	600, 630, 640 °C	MgO, Al_2MgO_4	[1]
Al–Cu/Al_2O_3	637 °C	Al_2O_3, and unknown phase	
Al–6.0 wt % Mg/Al_2O_3	800 °C	Al_2MgO_4	[6]
Al–3.0 wt % Mg/Al_2O_3	800 °C	No product	
Al–Mg/Al_2O_3	638–675 °C	Al_2MgO_4	[8]
Al–Mg/Al_2O_3	50 °C above the liquidus temp.	Al_2MgO_4	[9]
Al–Mg/Al_2O_3	150 °C above $T_{liquidus}$	No product	[10]
Mg/Al_2O_3	723 °C	Al_2MgO_4	[11]
Al–Mg/Al_2O_3	500 °C	MgO, Al_2MgO_4	[12]
Al–Mg/Al_2O_3	700, 750, 800, 850 °C	Al_2MgO_4	[13]
Al–Mg/Al_2O_3	675–800 °C	Al_2MgO_4	[14]
Al–7.4 wt % Mg/Al_2O_3	800 °C	Al_2MgO_4	Present work
Al–2.4 wt % Mg/Al_2O_3	800 °C	No product	Present work
Al–Cu/Al_2O_3	800 °C	Al_2O_3	Present work

TABLE II Interfacial reactions in the Al/Ni and Mg/Ni systems

System	Experimental condition	Experimental results	Reference
Al/Ni	400, 625 °C	Al_3Ni, Al_3Ni_2	[16]
Al/Ni	600 °C, 340 h	Al_3Ni, Al_3Ni_2, AlNi, $AlNi_3$	
Al/Ni	610 °C, 66 h	Al_3Ni, Al_3Ni_2	[18]
Al/Ni thin film	250 °C	Al_3Ni	[19]
Al/Ni thin film	400, 430 °C	Al_3Ni	[20]
Al/Ni thin film	220 °C	Al_3Ni, $AlNi_3$, unknown phases	[21]
Al/Ni	600, 700, 750 °C	Al_3Ni, Al_3Ni_2	Present work
Mg/Ni thin film	225 °C	Mg_2Ni	[22]
Mg/Ni	660, 680 °C	Mg_2Ni	Present work

and Rieck [18] also found only Al_3Ni, Al_3Ni_2 phases at the Al/Ni interface of the Al/Ni diffusion couples annealed at 610 °C up to 66 h. Nastasi *et al.* [19] and Bertoti *et al.* [20] observed the formation of Al_3Ni phase in the thin-film Al/Ni system. The thin-film study by Tarento and Blaise [21] indicated different results and they reported the formation of the Al_3Ni, $AlNi_3$ and other unknown phases at the Al/Ni interface. As listed in Table II, the above-mentioned results were all for solid aluminium and solid nickel systems, while analogous liquid diffusion couples studies regarding the molten aluminium and solid nickel were not found in the literature. Hong and d'Heurle [22] studied the Mg/Ni system and found Mg_2Ni phase at the Mg/Ni interface, but did not find the $MgNi_2$ phase. In this study, the interfacial reactions between the molten metals and plates were determined via the liquid diffusion couples experiments concerning the formation of intermetallic phases, the dissolution rates of the nickel plates, and the morphology of the interfaces. For comparison, a diffusion couple made of solid aluminium and solid nickel plate and annealed at 600 °C was also prepared in this study.

2. Experimental procedure

The aluminium alloys utilized in this study were prepared by using a conventional method as described previously [23] and were from pure aluminium, copper and magnesium elements of 99.999% purity. The compositions of the prepared alloys were analysed by using inductively coupled plasma (ICP), and the results are listed in Table III. Three different types of plate were used for preparing diffusion couples, and they were pure nickel plate (99.995% purity), pure alumina plate (polycrystalline, 99.5% purity), and nickel-plated alumina plate. The conventional electroless-plating procedures described in the Metals Handbook [24] were followed for the nickel plating of alumina. The thicknesses of the alumina plate, the nickel plate, and the electroless-plated nickel layer were 750, 1000 and 3 μm, respectively. The width and length of the plates were 0.4 and 2.3 mm, respectively.

TABLE III Compositions of the alloys used in this study

Alloy	Composition
1	Al–1.7 wt % Mg
2	Al–2.4 wt % Mg
3	Al–7.4 wt % Mg
4	Al–2.0 wt % Cu
5	Al–4.0 wt % Cu
6	Al–8.0 wt % Cu

As shown in Fig. 1, each plate was held vertically in a graphite crucible with two pieces of metal which weighed 3 g. The sample-containing crucible was loaded into a quartz tube and sealed in a 10^{-4} torr (1 torr = 133.322 Pa) vacuum. For diffusion couples of types 1–14, the sealed quartz capsules were kept inside a vertical furnace at a pre-determined temperature, and after a pre-set length of time they were

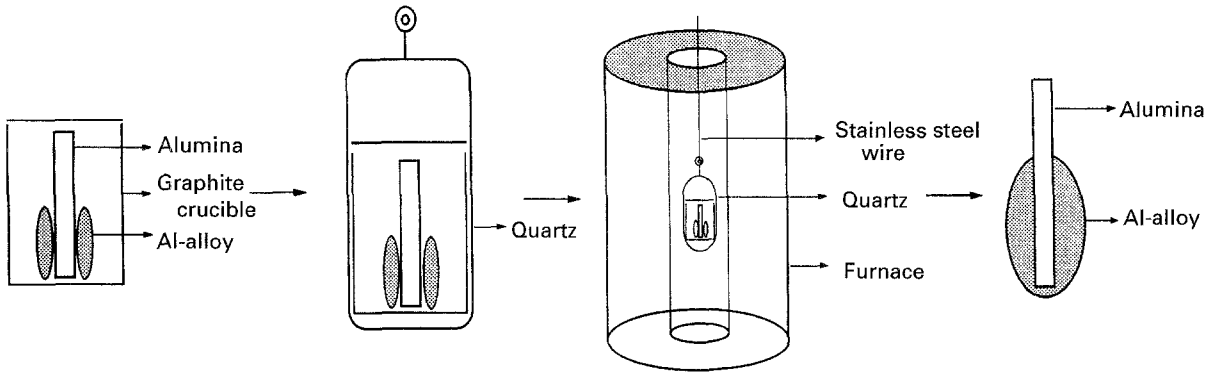

Figure 1 A schematic diagram of the diffusion couple preparation procedures.

taken out of the furnace and cooled in air. For diffusion couples of types 1, 2–8, 9–14, the annealing temperatures were 660 and 680 °C, 700 and 750 °C, and 800 °C, respectively. These annealing temperatures were higher than the melting points of aluminium (or magnesium) and its alloys, while lower than those of the nickel plate and the alumina plate. For diffusion couples of type 15, the sample capsules were first held at 700 °C for 5 min, and then were transferred to a furnace at 600 °C.

These air-cooled diffusion couple samples were first mounted and polished to reveal the cross-sections of the interfaces. The interfacial reactions in the diffusion couples were then analysed by using optical microscopy (OM), scanning electron microscopy (SEM) and electron probe microanalysis (EPMA). X-ray diffraction (XRD) was also used to identify the phases formed at the interfaces. Owing to the non-planar interfaces in the annealed diffusion couples, the thickness of the remaining nickel layer was measured and the average values of the thickness were reported. Because well-defined reaction zones were not found in the diffusion couples with alumina plates, a different examination technique was applied. The air-cooled diffusion couple samples with alumina plates were etched in a NaOH solution to remove the unreacted aluminium alloys and to reveal the interface, which was later analysed by using SEM and EPMA.

3. Results and discussion

3.1. Diffusion couples with nickel plate

In the beginning of the annealing process, the molten metal surrounded the nickel plate and formed the liquid diffusion couples; during the process, intermetallic phases nucleated and grew at the interface, and the nickel layer dissolved by diffusion through the intermetallic phases into the unsaturated molten metal. As shown in Fig. 2, a reaction layer was observed in type 1 diffusion couple, which was the molten magnesium with nickel plate. This reaction layer existed in all the type I diffusion couples annealed with various times and temperatures as listed in Table IV, and the layer was determined to be Mg_2Ni using energy-dispersive spectrometry (EDS) and XRD. The bright phase on the right-hand side of Fig. 2 was the unreacted nickel plate, while on the left-hand side was the two-phase mixture of magnesium and Mg_2Ni, and the mixture was liquid phase prior to solidification. According to the equilibrium Mg–Ni phase diagram [25], both Mg_2Ni and $MgNi_2$ phases are likely to form; however, the $MgNi_2$ phase was not observed in all the type I diffusion couples investigated in this study. The average thickness of the remaining nickel layer was measured, and thus the dissolution rates of nickel could be calculated, as shown in Fig. 3.

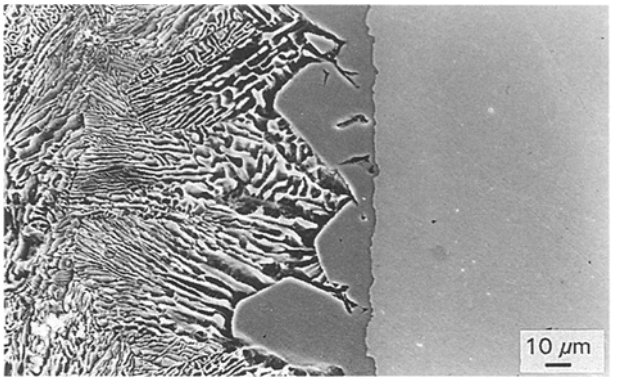

Figure 2 Microstructure of the interface in the Mg/Ni diffusion couple annealed at 680 °C for 10 min.

Two different reaction layers were found in all the type 2 diffusion couples, which were molten aluminium with nickel plate. As shown in Fig. 4, the layer adjacent to the nickel plate was the Al_3Ni_2 phase, while the layer next to it and adjacent to the liquid phase was the Al_3Ni phase. These phases were identified by using XRD and EDS. To achieve a more accurate analysis, the AlNi phase was prepared by using an arc-melter and served as a standard reference for the EDS analysis. The dissolution rates of the nickel plates were measured in terms of the layer's thickness, and are shown in Fig. 5. According to the Al–Ni equilibrium phase diagram [15], besides the Al_3Ni and Al_3Ni_2 phases, two other phases, AlNi and $AlNi_3$, should have formed in the diffusion couples annealed at 750 and 700 °C; however, the latter two phases were not observed. These results, which showed only some of the possible phases at the interfaces, were in agreement with those determined at lower temperatures both in the literature [16–20], and in this study, which was the type 15 diffusion couples exhibiting only Al_3Ni and Al_3Ni_2 phases at the interfaces.

TABLE IV Different types of diffusion couples

	Diffusion couple	Temp. (°C)	Time inside the furnace	Interfacial reactions
1	Mg/Ni plate	660, 680	5, 10, 15 min	Mg_2Ni
2	Al/Ni plate	700, 750	10, 20, 30 min	Al_3Ni, Al_3Ni_2
3	Alloy 1/Ni plate	700, 750	10, 20, 30 min	Al_3Ni (ε), Al_3Ni_2 (δ)
4	Alloy 2/Ni plate	700, 750	10, 20, 30 min	Al_3Ni (ε), Al_3Ni_2 (δ)
5	Alloy 3/Ni plate	700, 750	10, 20, 30 min	Al_3Ni (ε), Al_3Ni_2 (δ)
6	Alloy 4/Ni plate	700, 750	10, 20, 30 min	Al_3Ni (ε), Al_3Ni_2 (δ)
7	Alloy 5/Ni plate	700, 750	10, 20, 30 min	Al_3Ni (ε), Al_3Ni_2 (δ)
8	Alloy 6/Ni plate	700, 750	10, 20, 30 min	Al_3Ni (ε), Al_3Ni_2 (δ)
9	Alloy 1/(Ni) Al_2O_3 plate	800	24 h	–
10	Alloy 2/(Ni) Al_2O_3 plate	800	24 h	–
11	Alloy 3/(Ni) Al_2O_3 plate	800	24 h	$MgAl_2O_4$
12	Alloy 4/(Ni) Al_2O_3 plate	800	24 h	Al_2O_3
13	Alloy 5/(Ni) Al_2O_3 plate	800	24 h	Al_2O_3
14	Alloy 6/(Ni) Al_2O_3 plate	800	24 h	Al_2O_3
15	Al/Ni plate	600	1, 2, 3 wk	Al_3Ni, Al_3Ni_2
16	Alloy 1–6/Al_2O_3 plate	800	1, 4, 8, 24, 72 h	–

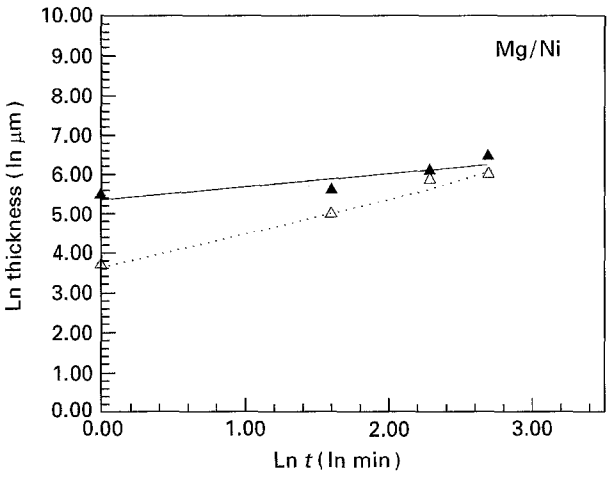

Figure 3 The average thickness of the nickel layer consumed by the interfacial reaction in the type 1 diffusion couple. (-▲-) 680 °C, (··△··) 660 °C.

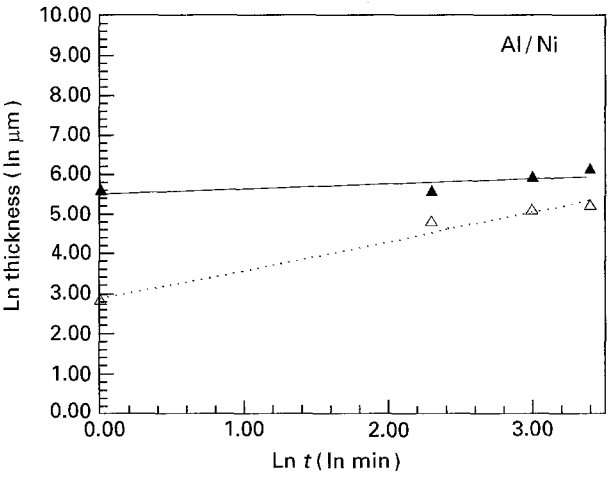

Figure 5 The average thickness of the nickel layer consumed by the interfacial reaction in the type 2 diffusion couple. (-▲-) 750 °C, (··△··) 700 °C.

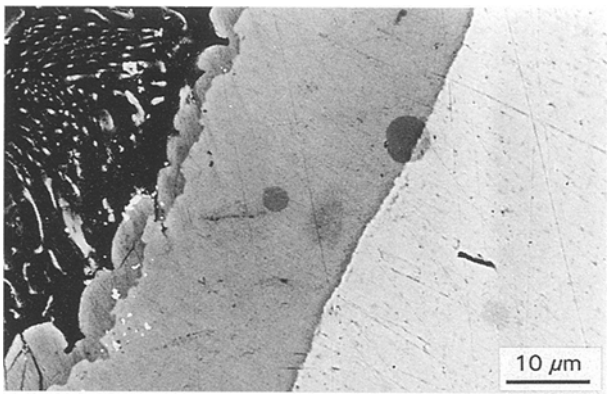

Figure 4 Microstructure of the interface in the Al/Ni diffusion couple annealed at 750 °C for 25 min.

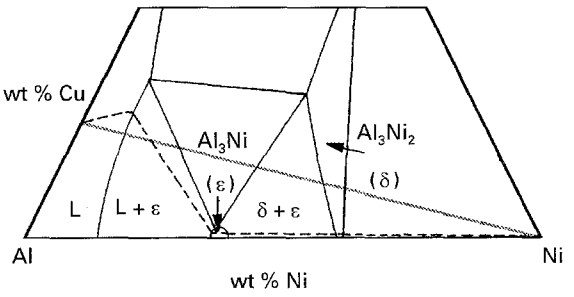

Figure 6 A schematic diagram of the diffusion paths of the Al–Cu/Ni diffusion couples in this study. (– – –) Diffusion path, (——) mass balance line.

The interfacial reactions determined in the diffusion couples types 3–8 were very similar to those observed in the type 2 diffusion couples. Two phases, Al_3Ni (ε) and Al_3Ni_2 (δ), formed at the interfaces. Their compositions were determined by using EDS and only a small amount of copper and magnesium was detected in the ε and δ phases. As shown in Fig. 6, a possible diffusion path of the Al–Cu/Ni system was determined by comparing the 700 °C isothermal section of the ternary Al–Cu–Ni [26] and the experimental results determined in this study. The diffusion paths of the Al–Mg/Ni and Al–Cu/Ni systems were similar and were determined to be liquid/Al_3Ni/Al_3Ni_2/Ni. The dissolution rates of nickel plates in the diffusion couples of types 3–8 are shown in Figs 7–12, respectively.

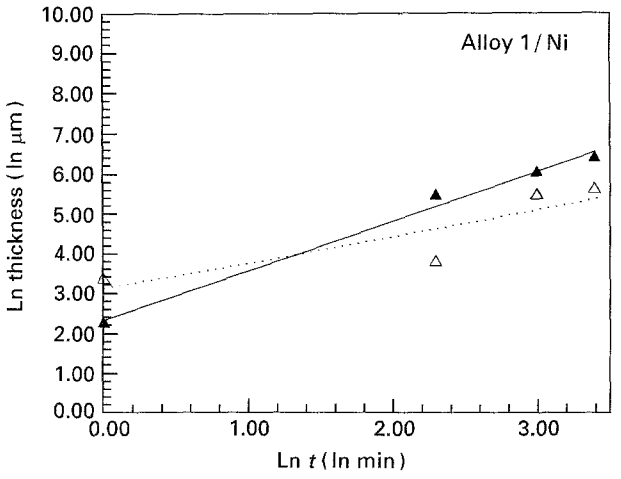

Figure 7 The average thickness of the nickel layer consumed by the interfacial reaction in the type 3 diffusion couple. (-▲-) 750 °C, (··△··) 700 °C.

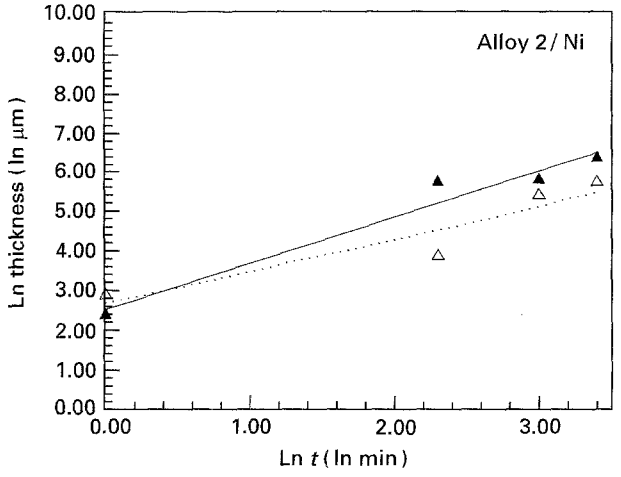

Figure 8 The average thickness of the nickel layer consumed by the interfacial reaction in the type 4 diffusion couple. (-▲-) 750 °C, (··△··) 700 °C.

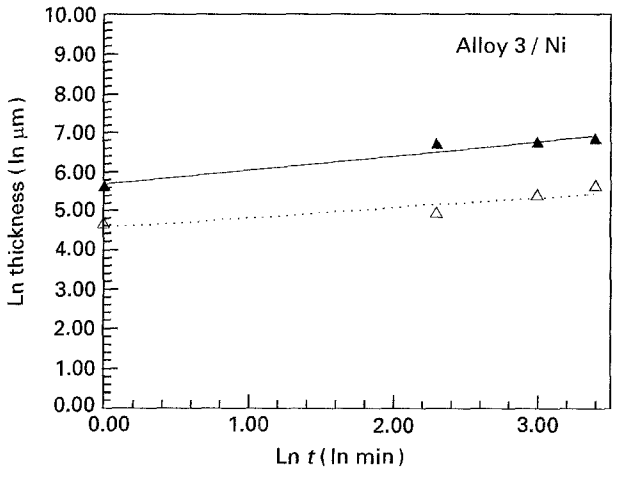

Figure 9 The average thickness of the nickel layer consumed by the interfacial reaction in the type 5 diffusion couple. (-▲-) 750 °C, (··△··) 700 °C.

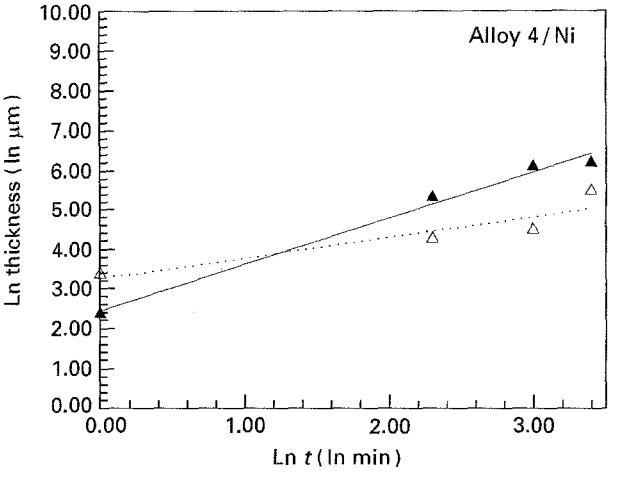

Figure 10 The average thickness of the nickel layer consumed by the interfacial reaction in the type 6 diffusion couple. (-▲-) 750 °C, (··△··) 700 °C.

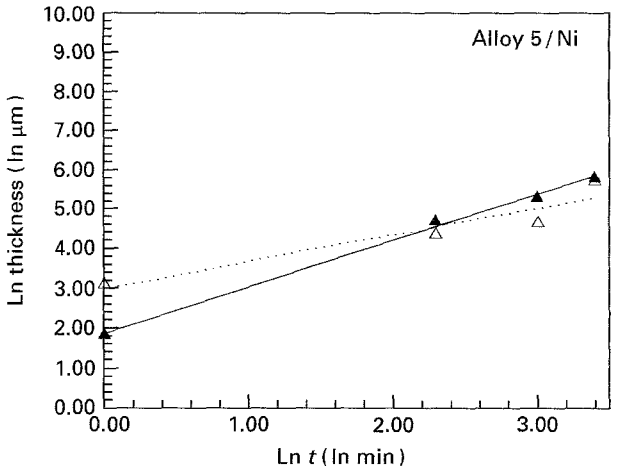

Figure 11 The average thickness of the nickel layer consumed by the interfacial reaction in the type 7 diffusion couple. (-▲-) 750 °C, (··△··) 700 °C.

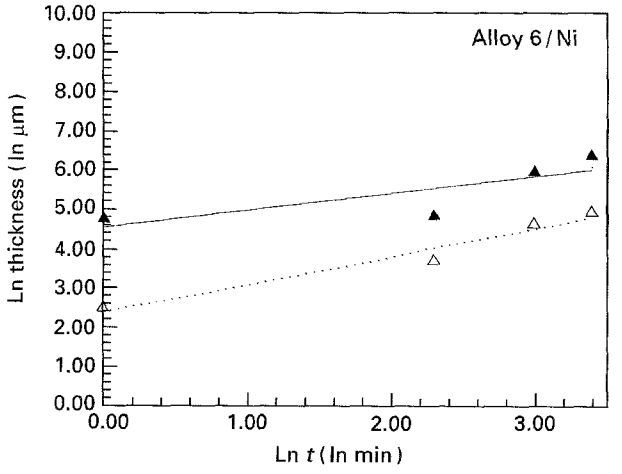

Figure 12 The average thickness of the nickel layer consumed by the interfacial reaction in the type 8 diffusion couple. (-▲-) 750 °C, (··△··) 700 °C.

The dissolution rates of the nickel plates, as shown in Figs 3, 5, and 7–12, were fitted to the following equation

$$\Delta X = A t^n \quad (1)$$

where ΔX is the thickness of the nickel layer consumed by the reaction, A is a constant, t the time for annealing, and n the empirical exponent. The values of n determined from the diffusion couples investigated

in this study are listed in Table V. If the rates of interfacial reactions were diffusion controlled, the value of n should have been 0.5, commonly called the parabolic law, whereas in this study the values of n varied from 0.16–1.21. Dybkov [27] indicated that if the reaction rate was interfacial reaction controlled, the rate was directly proportional to the reaction time, i.e. $n = 1$. This interfacial reaction control mechanism would then transit to diffusion control when the thickness of the reacted layer became large, i.e. $n = 0.5$. van Loo [28] and Old and Macphail [29] pointed out that several reasons could cause the deviation of the rate of layer growth from the parabolic law, such as the existence of the oxide layer. Kang and Ramachandran [30] noticed that the growth kinetics of the intermetallic phases at the liquid/solid interface changed during reaction. They found that the parabolic law was followed for both the initial ($n = 0.54$) and final stages (0.63), while the growth was slow in the intermediate stage ($n = 0.12$). However, because there were only four data points in every set of diffusion couple experiments, there are uncertainties in the values of n reported in this study, and further experimental investigations are needed. For all the liquid diffusion couples in this study, the morphology of the layers of the intermetallic phases adjacent to the molten metal was very faceted, while along the solid nickel interface it was planar, as can be noted in Figs 3 and 5. This faceted morphology was also reported in other systems in relation to the liquid–solid interfaces [29–33], while the morphology of the interface was mostly planar along the binary solid–solid interfaces [28]. Interfacial reactions between solid–solid are often encountered and have been intensively studied; however, the investigations of the interfacial reactions between liquid–solid are much less investigated [28, 30]. Further studies are needed to seek explanations for the different behaviours, primarily regarding the interfacial reaction rate and interfacial morphology.

TABLE V The empirical exponent n in the rate equation $\Delta X = A t^n$ for the nickel dissolution rates in the diffusion couples investigated in this study

Diffusion couple	Annealing temperature (°C)	n
1	660	0.87
1	680	0.32
2	700	0.78
2	750	0.16
3	700	0.68
3	750	1.26
4	700	0.84
4	750	1.19
5	700	0.29
5	750	0.39
6	700	0.55
6	750	1.21
7	700	0.7
7	750	0.19
8	700	0.73
8	750	0.45

3.2. Diffusion couples with alumina plate and nickel-plated alumina plate

A gap between the molten metal and the alumina plate was observed in all the diffusion couples with pure alumina plate. Several attempts, such as cleaning, preheating and degassing the alumina plate, were made but failed to improve this "non-wetting" situation. As expected, this "non-wetting" problem was overcome by using the nickel-plated alumina plate. The 3 μm thick electroless-plated nickel layer reacted with the molten metal and contributed to the rupture of the molten metal's surface oxide layer, which was believed to be the main obstacle to the molten metal wetting the alumina plate.

The Al_2MgO_4 spinel was found in the type 11 diffusion couples. The excessive amount of aluminium alloy in the annealed diffusion couple was removed by etching in the NaOH solution, and the surface of the alumina plate was then exposed. As shown in Fig. 13a,

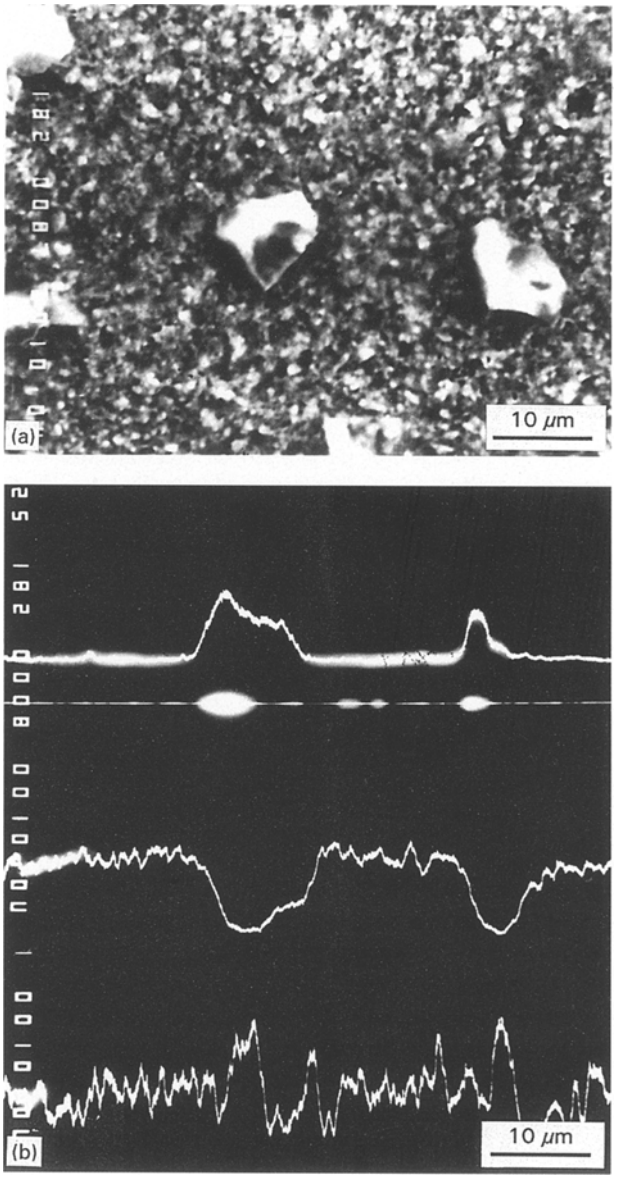

Figure 13 (a) Secondary electron image of the spinel grown in the type 11 diffusion couple annealed at 800 °C for 24 h. (b) From top to bottom are the X-ray elemental line scans of the magnesium, aluminium and oxygen, respectively and are across the centre of the exposed surface as shown in (a).

the ~ 10 μm particles were the Al_2MgO_4 spinel. The spinel phase was identified by using the qualitative X-ray elemental analysis and by comparing the morphology with those reported in the literature [13]. As shown in Fig. 13b, the results of the X-ray elemental line scans across the spinel particles, indicated an enrichment of the magnesium, oxygen and a depletion of aluminium in comparison with the alumina substrate. Spinel particles were not found in the type 9 and 10 diffusion couples. Weirauch [6] reported a similar observation, which indicated that spinel did not form in the Al–Mg/alumina interface when the content of magnesium was less than 6 wt % in the aluminium alloy. The secondary electron image of the surface of alumina plate in the as-received condition is shown in Fig. 14a, while larger particles were observed on the surface of alumina plate for diffusion couples 14 as shown in Fig. 14b. The elemental X-ray mapping and EDS analysis indicated that those particles were the Al_2O_3, and these results were in agreement with those determined by Levi *et al.* [1]. Similar results were also obtained for all the types 12–14 diffusion couples. The thermodynamic driving forces for the formation of the various phases, such as CuO, Al_2O_3, and Al_2CuO_4, at the interfaces were discussed by Levi *et al.* [1] and McLeod and Gabryel [14] previously; however, the formation of the CuO and Al_2CuO_4 phases was not found in any of the diffusion couples investigated in this study.

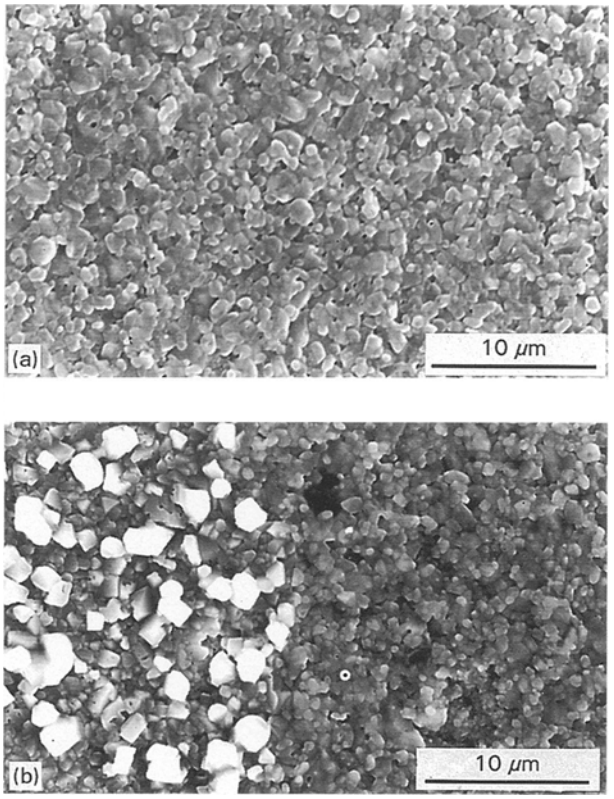

Figure 14 (a) Secondary electron images of the surface of (a) the alumina plate in the as-received condition, and (b) alumina in the type 14 diffusion couple annealed at 800 °C for 24 h.

4. Conclusion

In the diffusion couples study, nickel plates consumed and only some of the equilibrium phases formed at the interfaces. Mg_2Ni was found in the molten Mg/solid Ni diffusion couples, while Al_3Ni and Al_3Ni_2 were observed in the molten Al (alloy)/solid Ni diffusion couples. The diffusion paths for the aluminium-rich alloy/Ni systems at 700 and 750 °C were determined to be liquid/Al_3Ni/Al_3Ni_2/Ni. The spinel phase was noticed in the diffusion couples made of molten Al–7.4 wt % Mg and nickel-plated alumina plate, while it was not observed in other types of diffusion couples. Larger Al_2O_3 particles were found at the molten Al–Cu alloys and alumina plate interfaces. Although the morphology of most binary solid–solid interfaces was planar, the morphology of the interfaces along the liquid–solid was found to be faceted.

5. Acknowledgements

The authors wish to acknowledge valuable discussions with Professor S.-J. Lin in the Materials Science and Engineering Department of the National Tsin-Hua University and the financial support of the National Science Council of Taiwan through Grant NSC 83-0402-E-007-018.

References

1. C. G. LEVI, G. J. ABBASCHIAN and R. MEHRABIAN, *Metall. Trans.* **9A** (1978) 697.
2. M. M. SCHWARTZ, "Composite Materials Handbook" (McGraw-Hill, New York, 1984).
3. W. LEPKOWSKI, *G&EN* (1991) 4.
4. A. MORTENSEN and M. J. KOCZAK, *J. Metals* **45**(3) (1993) 10.
5. F. DELANNAY, L. FROYEN and A. DERUYTTERE, *J. Mater. Sci.* **22** (1987) 1.
6. D. A. WEIRAUCH, Jr, *J. Mater. Res.* **3** (1988) 729.
7. N. MORI, H. MIYAHARA, M. KOGA and K. OGI, *J. Jpn Inst. Metals* **55** (1991) 444.
8. A. MUNITZ, M. METZGER and R. MEHRABIAN, *Metall. Trans.* **10A** (1979) 1491.
9. B. F. QUIGLEY, G. J. ABBASCHIAN, R. WUNDERLIN and R. MEHRABIAN, *ibid.* **13A** (1982) 93.
10. G. R. CAPPLEMAN, J. F. WATTS and T. W. CLYNE, *J. Mater. Sci.* **20** (1985) 2159.
11. B. HALLSTEDT, Z.-K. LIU and J. AGREN, *Mater. Sci. Eng.* **A129** (1990) 135.
12. R. MOLINS, J. D. BARTOUT and Y. BIENVENU, *ibid.* **A135** (1991) 111.
13. C.-F. HORNG, S.-J. LIN and K.-S. LIU, *ibid.* **A150** (1992) 289.
14. A. D. McLEOD and C. M. GABRYEL, *Metall. Trans.* **23A** (1992) 1279.
15. P. NASH, M. F. SINGLETON and J. L. MURRAY, " ASM Handbook", Vol. 3, "Alloy Phase Diagrams", edited by H. Baker and H. Okamoto (ASM International, Materials Park, OH, 1992) p. 249.
16. L. S. CASTLEMAN and L. L. SEIGLE, *Trans. TMS-AIME* **209** (1957) 1173.
17. *Idem, ibid.* **212** (1958) 589.
18. M. M. P. JANSSEN and G. D. RIECK, *ibid.* **239** (1967) 1372.
19. M. NASTASI, L. S. HUNG and J. W. MAYER, *Appl. Phys. Lett.* **43** (1983) 831.
20. I. BERTOTI, M. MOHAI, A. CSANADY, P. B. BARNA and H. BEREK, *Surf. Interf. Anal.* **19** (1992) 457.
21. R. J. TARENTO and G. BLAISE, *Acta Metall.* **37** (1989) 2305.

22. Q. Z. HONG and F. M. d'HEURLE, *J. Appl. Phys.* **72** (1992) 4036.
23. S.-W. CHEN, C.-H. JAN, J.-C. LIN and Y. A. CHANG, *Metall. Trans* **20A** (1989) 2247.
24. W. D. FIELDS, R. N. DUNCAN and J. R. ZICKGRAF, "Metals Handbook", 9th Edn, Vol. 5, "Surface Cleaning, Finishing, and Coating" (ASM International, Materials Park, OH, 1985) pp. 219–43.
25. A. A. NAYEB-HASHEMI and J. B. CLARK, "ASM Handbook", Vol. 3, "Alloy Phase Diagrams", edited by H. Baker and H. Okamoto (ASM International, Materials Park, OH, 1992) p. 2.281.
26. W. KOSTER and K. MOELLER, *ibid.*, p. 3.11.
27. V. I. DYBKOV, *J. Mater. Sci.* **21** (1986) 3078.
28. F. J. J. van LOO, *Prog. Solid State Chem.* **20** (1990) 47.
29. C. F. OLD and I. MACPHAIL, *J. Mater. Sci.* **4** (1969) 202.
30. S. K. KANG and V. RAMACHANDRAN, *Scripta Metall.* **14** (1980) 421.
31. T. ISHIDA, *Trans. Jpn. Inst. Metals* **14** (1973) 37.
32. H. FIDOS and H. SCHREINER, *Z. Metallkde* **61** (1970) 225.
33. H. IKAWA, Y. NAKAO and T. ISAI, *Trans. Jpn. Welding Soc.* **10** (1979) 24.

Received 18 July 1994
and accepted 28 April 1995